JACS
JOURNAL OF THE AMERICAN CHEMICAL SOCIETY
pubs.acs.org/JACS
Article

Photochemical Ring-Opening Reaction of 1,3-Cyclohexadiene: Identifying the True Reactive State

Oksana Travnikova,[○] Tomislav Piteša,[○] Aurora Ponzi, Marin Sapunar, Richard James Squibb, Robert Richter, Paola Finetti, Michele Di Fraia, Alberto De Fanis, Nicola Mahne, Michele Manfredda, Vitali Zhaunerchyk, Tatiana Marchenko, Renaud Guillemin, Loic Journel, Kevin Charles Prince, Carlo Callegari, Marc Simon, Raimund Feifel, Piero Decleva, Nađa Došlić,* and Maria Novella Piancastelli*

Cite This: J. Am. Chem. Soc. 2022, 144, 21878−21886
Read Online
ACCESS | Metrics & More | Article Recommendations | Supporting Information

ABSTRACT: The photochemically induced ring-opening isomerization reaction of 1,3-cyclohexadiene to 1,3,5-hexatriene is a textbook example of a pericyclic reaction and has been amply investigated with advanced spectroscopic techniques. The main open question has been the identification of the single reactive state which drives the process. The generally accepted description of the isomerization pathway starts with a valence excitation to the lowest lying bright state, followed by a passage through a conical intersection to the lowest lying doubly excited state, and finally a branching between either the return to the ground state of the cyclic molecule or the actual ring-opening reaction leading to the open-chain isomer. Here, in a joint experimental and computational effort, we demonstrate that the evolution of the excitation−deexcitation process is much more complex than that usually described. In particular, we show that an initially high-lying electronic state smoothly decreasing in energy along the reaction path plays a key role in the ring-opening reaction.

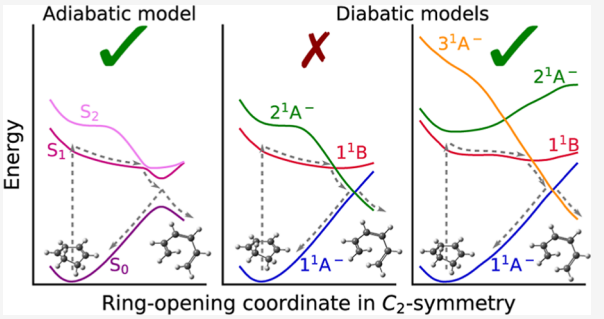

INTRODUCTION

The photochemical ring-opening reaction of 1,3-cyclohexadiene (CHD) to 1,3,5-hexatriene (HT) is a textbook example of a pericyclic reaction.[1,2] In addition to many theoretical investigations,[3−13] the dynamical evolution of photoexcited CHD has been studied, possibly more than any other photochemical reaction, with a large variety of spectroscopic techniques for isolated molecules, that is in collision-free conditions and without solvent effects (see e.g., refs 14−22). This pronounced interest arises from the fundamental importance of the reaction, its biological relevance,[23,24] and a range of applications in organic synthesis and materials science.[25−29]

The conceptual framework to understand the photochemistry of CHD is provided by the Woodward−Hoffmann rules,[30] extended by van der Lugt and Oosterhoff,[31,32] stating that the conrotatory ring-opening reaction is mediated by a doubly excited electronic state of the same symmetry as the ground state (1^1A^-). In the ring-opening reaction, the lowest unoccupied molecular orbital of CHD, which is doubly occupied in the reactive state, becomes the highest occupied molecular orbital of HT. The generally accepted sequence of events starts with a valence excitation by a wavelength of about 267 nm to the first (S_1) bright state, labeled 1^1B, followed by a passage through a conical intersection (CoIn) to a dark state, labeled 2^1A^-. The following step is a branching between two pathways at a second CoIn, either the return to the ground state of the cyclic molecule or the actual ring-opening reaction leading to the open-chain isomer (see e.g. ref 11−15). It is noticed that the labels above and throughout the text indicate diabatic states and that we use the notation for alternant π-system (plus and minus) pseudosymmetry.[33,34]

In general, photochemical reactions are assumed to be driven by CoIns at which two adiabatic Born−Oppenheimer potential energy surfaces (PESs) become degenerate and which act as effective funnels for the transfer of population between different adiabatic PESs.[35−37] In contrast to adiabatic PESs, which suddenly change their chemical character near a CoIn, PESs that retain their character and cross at CoIns are known as diabatic states. As properties such as the electronic transition dipole moment change smoothly only in the diabatic

Received: June 15, 2022
Published: November 29, 2022

https://doi.org/10.1021/jacs.2c06296
J. Am. Chem. Soc. 2022, 144, 21878−21886

representation, the dynamics of the diabatic electronic population is the one monitored in time-resolved ultrafast spectroscopy.[38−41]

Despite tremendous efforts, a conclusive proof of the reactivity of the diabatic 2^1A^- state has not yet been achieved. To address this problem, we ask a seemingly simple question: is there any other electronic state of symmetry A and partial double excitation character that may be involved in the ring-opening reaction in CHD? Here, in a joint experimental and computational effort, we show that the evolution of the process is more complex than that usually described. In particular, we show that a high-lying state with a pronounced double excitation character, labeled 3^1A^-, plays a key role in the ring-opening reaction.

To observe the first stages of a photochemical process, a suitable method is to prepare a photoexcited state with an optical laser, the so-called pump, and then follow its evolution by valence photoelectron spectroscopy, the so-called probe, as a function of pump−probe time delay, with resolution on the picosecond (ps, 10^{-12} s) or femtosecond (fs, 10^{-15} s) timescale. Time-resolved photoemission is the first-choice technique to follow the evolution of a system as it provides information on both electronic and nuclear dynamics. Furthermore, it provides information on states which are not reachable by absorption methods, in particular dark states, which need to be characterized in the present case.

A breakthrough in this direction is represented by the FERMI free-electron laser (FEL) at the Elettra facility, Trieste, Italy. Time-resolved photoemission spectra can be obtained here with the spectral resolution high enough to precisely characterize ionization from electronic states even if they are weak and/or close in energy (see e.g., refs 42 and 43). FERMI, as a seeded FEL, offers the advantages of a narrow photon energy bandwidth, negligible photon energy jitter, higher stability, higher pulse energies, and much higher photon fluxes with respect to monochromatized sources based on high harmonic generation.

RESULTS AND DISCUSSION

Our experiments were performed at FERMI at the Low Density Matter (LDM) beamline, devoted to atomic and molecular spectroscopy studies.[44] The pump was a titanium−sapphire optical laser, providing a wavelength of 267 nm, and the probe was valence photoelectron spectroscopy with a photon energy of 19.23 eV. The delay time range was from −1 to 2 ps, spanned in steps of 50−100 fs. We recorded the valence photoelectron spectra with a magnetic bottle spectrometer[45,46] (see Supporting Information, SI, for further details on the facility, the beamline, and the spectrometer).

In the upper panels (experiment and theory) of Figure 1, we show the valence photoelectron spectra recorded for several values of pump−probe delay in the delay range from −1 to 2 ps in steps of 100 fs. The spectra are plotted as a two-dimensional map, highlighting the variations in spectral intensity as a function of time delay. The ground-state spectrum is subtracted from the spectra obtained at later times (see Supporting Information and Figures S2−S4 for further details on how the experimental spectra are obtained). The upper panels illustrate the variations of the photoionization signal as a function of the pump−probe delay, and the changes of averaged signals in the four characteristic areas are shown in the lower panels (experiment and theory). We notice the development of a series of new features in two

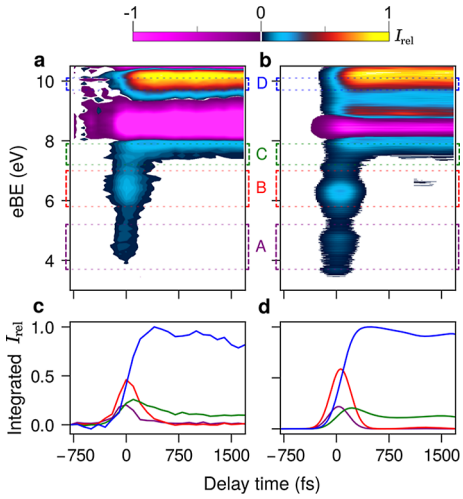

Figure 1. (a) Experimental and (b) computed differential 2D maps of the photoelectron spectra of CHD. White color denotes the regions with $|I_{rel}| < 0.01$. For the computed excited-state absorption component of the signal (separated on CHD- and HT-ending trajectories), check Figure S5. (c) Experimental and (d) computed time evolution of the spectral intensity integrated over the area marked by colored rectangles in (a). For experimental and computational details, see the Supporting Information.

electron energy regions, that is, at a low binding energy (4−8 eV) and around 10 eV. The low-binding-energy region is characteristic of spectral features related to excited states or dynamical features due to the photoexcitation process, while the 10 eV region is in the range characteristic of ground-state features.

The three features in the low-binding-energy region have a different behavior as a function of delay: the two peaks at 4.5 and 6.4 eV binding energies reach maxima at 0 ps and decrease to zero intensity after 0.5 ps, while the third feature at 7.5 eV has a low intensity at 0 ps, continues to grow to a maximum at 0.5 ps, and finally stabilizes after about 1 ps. The feature at a high binding energy, 9.9 eV, grows after 0 ps as a function of delay and stays constant after about 0.5 ps. We denote these features A, B, C, and D in the order of increasing binding energy. The disappearing features A and B "feed" the developing ones C and D, giving evidence of a dynamical change accompanying the electronic relaxation. This is a first hint that features A and B correspond to excited states which relax on a femtosecond timescale, while the features C and D that develop and then reach an asymptotic value are connected to the electronic states belonging to vibrationally hot open chain and/or closed ring isomers.

This assignment is strongly supported by theory. The photoinduced dynamics was simulated with nonadiabatic surface-hopping trajectories. In this method, an ensemble of classical trajectories is propagated starting from the excited state, and the stochastic fewest switches algorithm[47] is used to allow each trajectory to "hop" to different electronic states based on the nonadiabatic couplings. A total of 107 trajectories were propagated for 1000 fs, with a time step of 0.5 fs in a manifold of three electronic states. The energies and forces needed for the propagation of the trajectories are computed using the (XMS(3)-CASPT2(6,6)) method, whose accuracy was assessed in ref 12 (see the Computational Section and Supporting Information for details).

https://doi.org/10.1021/jacs.2c06296
J. Am. Chem. Soc. 2022, 144, 21878−21886

The photoelectron spectra were computed in the sudden approximation in which the partial cross sections are approximated with Dyson orbital norms.[48−50] The accuracy of the sudden approximation was assessed by comparison with the benchmark spectrum computed using a B-spline description of the photoelectron continuum[51,52] (see Figure S6). To match the experiment, the theoretical spectra have been shifted by +0.3 eV. For further details on how the theoretical spectra are calculated, see the Methods section and Supporting Information. The agreement between the experimental and simulated spectra is remarkably good, both in terms of intensity and time evolution of the peaks, with the width of the ground-state bleach component (purple) being the only major discrepancy. The simulated spectra, when analyzed separately for nonreactive (CHD) and reactive (HT) trajectories (see Figure S5), show that band C arises mainly from the vibrationally hot CHD, while band D is primarily due to the newly formed HT molecules. The latter assignment is confirmed by a comparison between the ground-state valence photoelectron spectra of CHD and HT, where there is spectral intensity in the binding energy region around 10 eV only for the open-chain isomer.[53,54]

While the assignment of features C and D is rather straightforward, the behavior of features A and B, which correspond to the excited states and therefore are the key to identify the true reactive one, is more complex. A first hint of the three-state model reported in the literature being oversimplified is that we do not observe a simple series of few peaks growing and decreasing in temporal sequence, as, for example, was reported in ref 42 for acetylacetone, where the adiabatic description was sufficient.

To fully explain the mechanism of the reaction, we need to connect the evolution of the photoionization bands as a function of time with the population of the diabatic electronic states involved in the reaction. To this end, we first consider the properties of the electronic states at the Franck−Condon geometry. The electronic spectrum of CHD reported in the literature is composed of two broad bands at ∼5.0 and ∼8.0 eV.[55] The first encompasses the bright $1^1A^- \rightarrow 1^1B$ and dark $1^1A^- \rightarrow 2^1A^-$ transitions. The second or *cis*-band is characteristic for *cis*-polyenes. Here, two valence transitions of mixed character have been identified—the intense $1^1A^- \rightarrow 1^1A^+$ transition at 8.0 eV[4,56] and a higher lying transition with a considerable vibronic structure.[55] Intercalated between these two bands are several sharp Rydberg transitions.[4,57] Owing to their weak coordinate dependence, Rydberg states are expected to play a negligible role in the ring-opening reaction.[58]

Vertical excitation energies of the six lowest valence excited states of CHD with the coefficients of the leading configuration state functions (CSFs) are collected in Table 1 (for EOM-CC3, results see Table S1), while the orbitals constituting the active space are illustrated in Figure S7.

The main results are summarized in Figure 2. At the Franck−Condon geometry, the XMS(7)-CASPT2[6e, 6o] method yields the 1^1B state at 5.18 eV, the dark 2^1A^- state at 5.99 eV, and the two bright states of the *cis*-band, 1^1A^+ and 3^1A^-, at 8.31 and 8.66 eV, respectively. The electron density differences between the excited states and the ground state plotted in Figure 2a show that excitation to the 1^1B and 3^1A^- states leads to the depletion of electron density on the C_1-C_6 bond, while excitation to 2^1A^- and 1^1A^+ leaves the density on that bond nearly unchanged. From the wave functions of the three states of symmetry A, which are dominated by the three

Table 1. State Ordering and Vertical Excitation Energies (in eV) of the Six Lowest Valence-Excited States at the Franck−Condon Geometry Labeled According to Plus−Minus Alternancy Symmetry, Leading CSFs and Their CI Coefficients Being Calculated at the XMS(7)-CASPT2[6e,6o] Level of Theory[a]

state	E/eV (f)	exp.[b] E/eV	leading CSFs	CI coeff.
1^1A^-			Aufbau	0.96
			$\pi_2\pi_2 \rightarrow \pi_1^*\pi_1^*$	−0.14
1^1B	5.18 (0.017)	4.94	$\pi_2 \rightarrow \pi_1^*$	0.97
2^1A^-	5.99 (0.008)		$\pi_2\pi_2 \rightarrow \pi_1^*\pi_1^*$	0.53
			$\pi_1 \rightarrow \pi_1^*$	−0.55
			$\pi_2 \rightarrow \pi_2^*$	0.46
2^1B	7.50 (0.007)		$\sigma \rightarrow \pi_1^*$	0.97
1^1A^+	8.31 (0.321)	7.90	$\pi_1 \rightarrow \pi_1^*$	0.69
			$\pi_2 \rightarrow \pi_2^*$	0.65
			$\pi_2\pi_2 \rightarrow \pi_1^*\pi_1^*$	0.16
3^1A^-	8.66 (0.217)		$\pi_2\pi_2 \rightarrow \pi_1^*\pi_1^*$	0.68
			$\pi_2 \rightarrow \pi_2^*$	−0.51
			$\pi_1 \rightarrow \pi_1^*$	0.28
3^1B	10.11 (0.000)		$\pi_1 \rightarrow \pi_2^*$	0.96

[a]For EOM-CC3 states, see Table S1. [b]Optical and electron energy loss spectroscopies.[56]

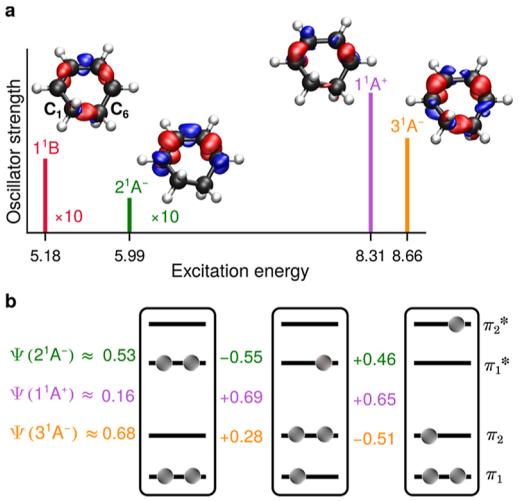

Figure 2. (a) Excitation energies and relative absorption intensities of the 1^1B, 2^1A^-, 1^1A^+, and 3^1A^- states (sticks) and the corresponding maps showing the electron density difference with respect to the electronic ground state calculated at the Franck−Condon geometry. Areas of increased and reduced electron densities are shown in blue and red, respectively. (b) Three valence states, 2^1A^- (green), 1^1A^+ (purple), and 3^1A^- (orange), with the CI coefficients of the three dominant CSFs ($\pi_2\pi_2 \rightarrow \pi_1^*\pi_1^*$, $\pi_1 \rightarrow \pi_1^*$, and $\pi_2 \rightarrow \pi_2^*$).

CSFs shown in Figure 2b, it is evident that the 3^1A^- state has a pronounced double excitation character (see CI coefficients) and the overall electronic properties of a potentially reactive state.

Figure 3 shows the one-dimensional potential energy profiles of the adiabatic (black) and diabatic (colors) states along the ring-opening path in C_2 symmetry. The diabatization has been performed on the basis of the lowest six adiabatic states by minimizing the variation of their wave functions along the reaction path.[59] The diabatization on the usual basis of the three lowest diabatic states, as defined at the FC geometry, is shown in Figure S8 (see also Figure S9). Details of the

https://doi.org/10.1021/jacs.2c06296
J. Am. Chem. Soc. 2022, 144, 21878−21886

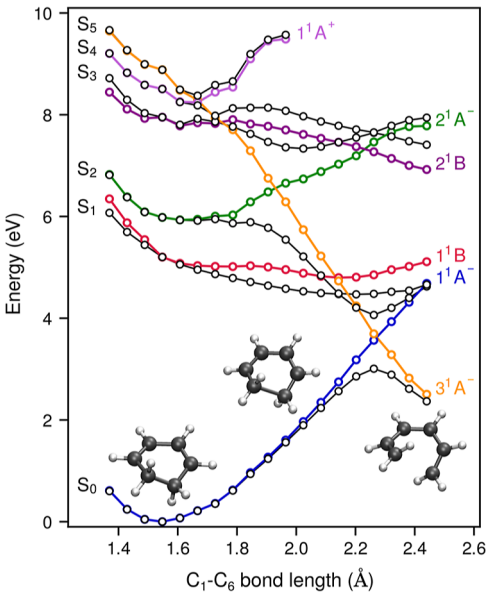

Figure 3. Coordinate dependence of the potential energy of the lowest adiabatic electronic states (black) and diabatic electronic states: 1^1A^- (blue), 1^1B (red), 2^1A^- (green), 2^1B (dark violet), 1^1A^+ (light violet), and 3^1A^- (orange). For comparison with the traditional three-state model, see Figure S8.

procedure are given in the Supporting Information. One sees that the coordinate dependence of the diabatic 1^1B state (red) matches the expected behavior, but this is not the case for the 2^1A^- state (green), which clearly increases in energy (destabilizes) along the reaction path. The diabatic 3^1A^- state (orange) is the state that is strongly stabilized in the reaction. The two states cross at $R(C_1{-}C_6) \sim 1.9$ Å where the adiabatic S_2 state shows the characteristic inflection. Further down the reaction path, 3^1A^- crosses with the 1^1B state and at $R(C_1{-}C_6) \sim 2.3$ Å with the ground state. This indicates that the ground state of HT correlates with the 3^1A^- state and not with the 2^1A^- state. Notice that the proposed pathway does not contradict the Woodward–Hoffmann rules as they do not prescribe that the reaction should proceed on the lowest doubly excited state at the FC geometry.

To understand the role of the different diabatic states in the ring-opening reaction when the C_2 symmetry is lifted, we analyze two representative nonadiabatic trajectories yielding CHD (Figure 4a–c) and HT (Figures 4d–4f). For additional trajectories, see Figure S10. The two trajectories exhibit a very similar behavior up to the CoIn with the ground state. In both cases, the dynamics is initiated in the S_1 state (Figure 4a,d), which is in the diabatic 1^1B state (Figure 4b,e). At two instances, at ~10 and ~25 fs, the gap between the S_1 and S_2 states becomes vanishingly small, and the S_1 state has a possibility to change its character.

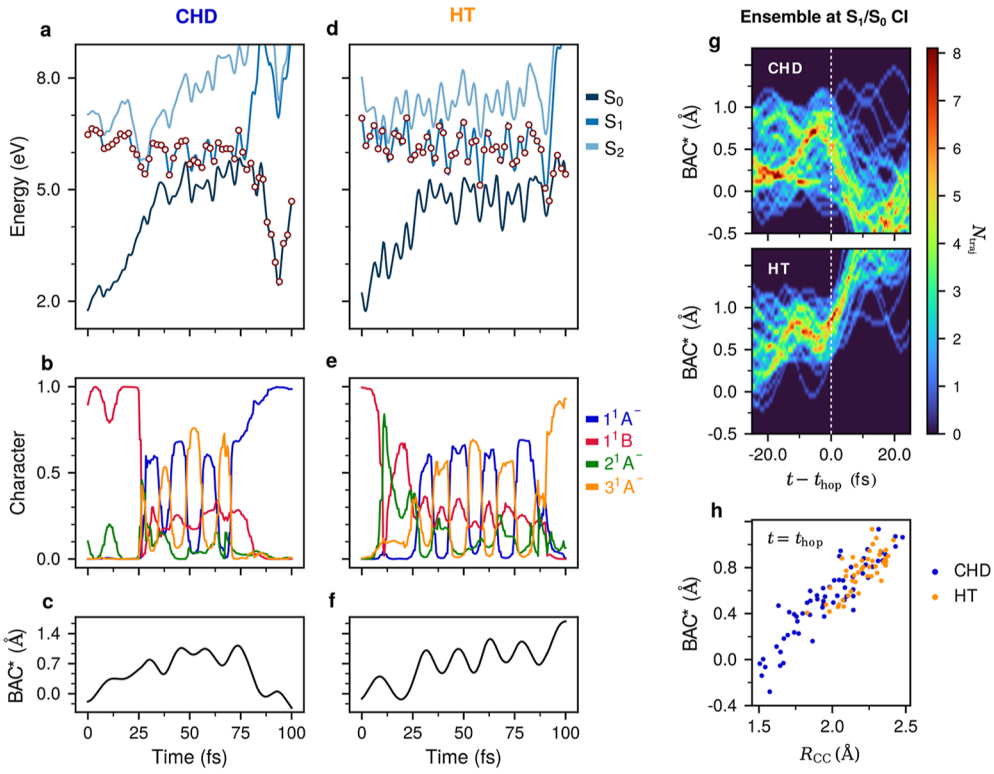

Figure 4. Two representative nonadiabatic trajectories leading to CHD (a–c) and HT (d–f). (a,d) Time evolution of the potential energy of the electronic ground state S_0 (dark blue) and the two lowest excited states S_1 (blue) and S_2 (light blue). Dots mark the instantaneous populations of electronic states. (b,e) Decomposition of the currently populated state in terms of four diabatic states, 1^1A^- (blue), 1^1B (red), 2^1A^- (green), and 3^1A^- (orange), along the trajectories. (c,f) Time evolution of the BAC* along the nonadiabatic trajectories. (g) Evolution of the BAC* coordinate for the ensemble of nonadiabatic trajectories synchronized to reach the S_1/S_0 CoIn simultaneously at $t' = t - t_{hop} = 0$. At the moment of hop, BAC* decreases for CHD and increases for HT trajectories. For the evolution of the $R(C_1{-}C_6)$ coordinate and relative velocity, $dR(C_1{-}C_6)/dt$, see Figure S13. (h) Distribution of $R(C_1{-}C_6)$ and BAC* at the moment of hop to S_0. Orange (blue) circles correspond to HT (CHD) trajectories. For other structural parameters, see Figure S14.

https://doi.org/10.1021/jacs.2c06296
J. Am. Chem. Soc. 2022, 144, 21878–21886

Indeed, the diabatic populations show a brief increase of the 2^1A^- contribution at ~10 fs (green), but then the 1^1B character is recovered until ~25 fs when its contribution suddenly drops. From ~25 fs onward, the S_1 state is best described as a superposition of the 1^1A^- (blue) and 3^1A^- (orange) diabatic states. The two states are strongly coupled by nuclear motion along the so-called extended bond-alternating coordinate (BAC*), which is the difference of single and double bond lengths in HT plus $R(C_1-C_6)$.[11] In the CHD trajectory, the return to the ground state occurs after a BAC* local maximum, while the C_1-C_6 bond is compressing and the S_1 state is dominantly of 1^1A^- character. On the contrary, in the HT trajectory, the CoIn with the ground state is encountered after a BAC* local minimum, while the C_1-C_6 bond is expanding and the S_1 state is dominantly of 3^1A^- character. After the hop, the CHT trajectory continues to evolve in the 1^1A^- state, and the HT trajectory continues to evolve in the 3^1A^- state, which is now the ground state leading to the HT product. Altogether, our analysis suggests that the fate of a nonadiabatic trajectory is determined by the character of the S_1 state at the moment of the $S_1 \rightarrow S_0$ nonadiabatic transition. If the transition occurs when the S_1 state has a dominant 1^1A^- character, the CHD product is formed and, vice versa, if the hop occurs when the S_1 state has a dominant 3^1A^- character, the HT product is formed. The analysis of the ensemble of nonadiabatic trajectories, divided in two groups, CHD and HT, and synchronized in such a way as to reach the S_1/S_0 CoIn at the same time, is given in Figure 4g,h. Figure 4g shows that for all HT trajectories BAC* increases before the hop to S_0, while it decreases for most but not all CHD trajectories. The distribution of $R(C_1-C_6)$ and BAC* at the time of hop (Figure 4h) indicates that for large BAC* and $R(C_1-C_6)$ distances, both CHD (blue) and HT (orange) can be formed in a close to 50:50 ratio, but for small BAC* and short $R(C_1-C_6)$, only CHD is formed, irrespective of whether BAC* is compressing or not. A closer inspection reveals that in this group of nonreactive trajectories, the population of the 3^1A^- state is negligibly small (see Figure S11), meaning that the existence of a second nonreactive pathway from either 1^1B or 2^1A^- cannot be excluded. We can now relate the average adiabatic and diabatic electronic populations to the time evolution of the two lowest energy bands in the photoelectron spectra. Figure 5a shows the two-dimensional map of theoretical photoelectron spectra at short delay times, as computed using eq 4 in the Supporting Information (without broadening the calculated signal to match the experimental resolution).

Two bands are clearly visible in the binding energy range of 3–7 eV. Band A starts at ~3.2 eV, and within 15 fs reaches a plateau at ~4.5 eV. It arises from the $S_1 \rightarrow D_0$ transition. The increase of the ionization energy is caused by the motion toward the minimum of the S_1 state. As this motion leads to the extension of the C_1-C_6 bond, the energy of the ground state of the CHD cation (D_0) increases (see Figure S12). At around ~30 fs, the band loses intensity. Band B starts at ~7.0 eV, but it is almost immediately stabilized to the 5.8–6.2 eV binding energy range. The sudden stabilization of band B is caused by the crossing of the cationic D_1 and D_2 states (see Figure S9). The maximum of the intensity of band B is reached at ~40 fs. Figure 5b shows the average population of the adiabatic states S_0, S_1, and S_2, as obtained from nonadiabatic dynamics simulations. By comparing the time evolution of bands A and B with the average population of the adiabatic

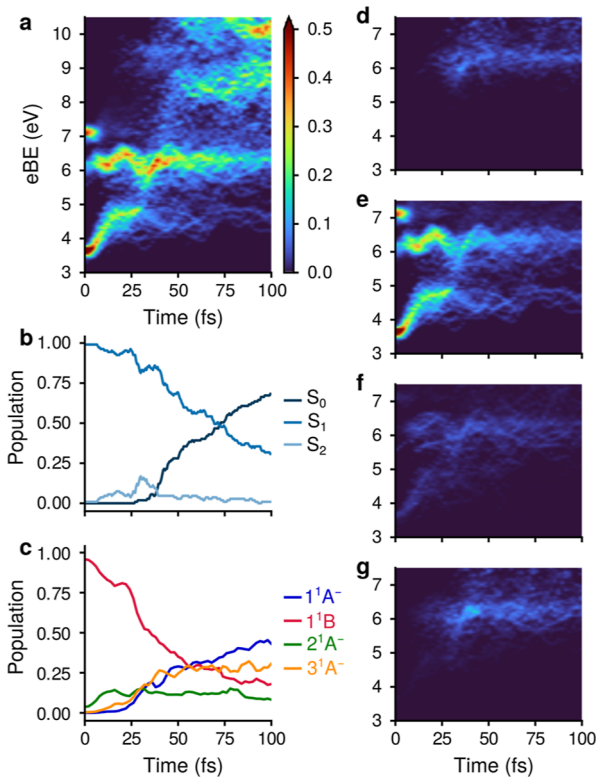

Figure 5. (a) Unconvoluted photoelectron spectra for short delay times. The ground-state bleach component is not taken into account. (b) Time evolution of the adiabatic population of electronic states obtained from surface-hopping nonadiabatic dynamics simulations. (c) Time evolution of the diabatic population of electronic states obtained by diabatization of electronic states along nonadiabatic trajectories. (d–g) Decomposition of the photoionization spectrum in terms of contributions of the diabatic states 1^1A^- (d), 1^1B (e), 2^1A^- (f), and 3^1A^- (g).

states, one sees that the loss of intensity of band A coincides with the transfer of population from the S_1 to the S_2 state, with the maximum at ~30 fs, while the maximum of the intensity of band B at ~40 fs coincides with the rather counterintuitive rise of the population of the S_0 state. The electronic populations of the diabatic states (Figure 5c) provide a more consistent view. The population initially residing in the 1^1B state steadily decreases. The 2^1A^- state is transiently populated at early times, but its population never exceeds 0.2. In the ~35–55 fs interval, the population of the 1^1A^- (blue) and 3^1A^- (orange) states increases, and the system evolves in a superposition of these two states. This interval coincides with the maximum of the intensity of band B. The decomposition of the photoelectron spectra into the contributions from the diabatic states in Figure 5d–g unambiguously shows that the increase of the intensity of band B at around 40 fs originates from the population of the 3^1A^- state (Figure 5g). As the reaction proceeds, the formation of the CHD and HT products correlating with the 1^1A^- and 3^1A^- states, respectively, becomes clearly visible.

Our analysis clearly points toward a predominant role of the 3^1A^- diabatic state in the reactive path and, in general, that a more consistent picture of the overall dynamics can be achieved by analyzing diabatic rather than adiabatic contributions. We consider these findings as a step forward with respect to the description usually reported in the literature.[11−22] We

https://doi.org/10.1021/jacs.2c06296
J. Am. Chem. Soc. 2022, 144, 21878−21886

rely on both experimental advances, such as the possibility of measuring time-resolved valence photoelectron spectra with rather high electron energy resolution, and theoretical methods allowing accurate calculations of the photoelectron signal and on-the-fly adiabatic-to-diabatic transformation of electronic populations.

To draw a comprehensive picture of the ring-opening mechanism, we consider previously reported results and compare them to our results. From the experimental side, our time-resolved valence photoelectron spectra measured with high electron kinetic energy resolution do not contradict the previously reported results, such as, for example, those obtained with transient absorption spectroscopy[15] and valence photoelectron spectroscopy with EUV pulses[20] to quote previous works in which the probe was an electronic structure technique. The ring-opening reaction in CHD was previously modeled with a variety of computational approaches including reaction path calculations,[3,6,60−62] wave packet simulations on reduced dimensionality PESs,[7,63−65] full-dimensional ab initio multiple spawning,[19,66,67] and surface hopping mixed quantum-classical dynamics.[9−13,20] From SH simulations, it emerges that the dynamics proceeds dominantly on the lowest adiabatic surface, takes place on a sub-100 fs timescale, and leads to HT production with a yield slightly lower than 50%. This is in good agreement with our results. Larger differences are found with respect to density functional theory (DFT)-based studies of Schalk et al.[11] in which a significantly larger quantum yield for HT production (64%) was obtained and of Filatov et al.[13] in which a significantly longer decay constant ($\tau \sim 235$ fs) of the S_1 state was predicted.

Concerning the photochemical mechanism, the commonly accepted mechanism—photoexcitation to the 1^1B state, internal conversion to the 2^1A^- state, and then CHD/HT bifurcation at $2^1A^-/1^1A^-$ CI—was challenged by Schalk el al.[11] The authors performed SH simulations in the S_1 state using TDDFT, that is, with a method that cannot describe states with double excitation character, and nevertheless obtained HT with a high quantum yield. On these grounds, the authors proposed that an adiabatic description, in which a single electronic state gradually changes character along the reaction path, was adequate and that a doubly excited state was not necessarily involved in the ring-opening reaction. This assumption was not justified by the subsequent high-level XMS-CASPT2 simulations of Polyak et al.,[12] where the authors reported that the double excitation character of 2^1A^- contributes to the nature of the S_1 and S_2 states at the minimal energy S_1/S_2 CI as well as afterward. The recent combined experimental and theoretical study of Karashima and co-workers[20] confirmed that two electronic states are involved in the reactions. They decomposed the two-dimensional maps of photoelectron spectra in contributions from two states, denoted S_1* and S_1**, but did not assign explicit diabatic labels to these states. However, as only two diabatic states, 1^1B and 2^1A^-, were discussed in ref 20, the reader was left with the implicit assumption that the reactive S_1** corresponds to the doubly excited 2^1A^- state.

In this work, we have performed an adiabatic-to-diabatic transformation on top of surface hopping simulations in which seven diabatic states have been included. Our analysis revealed that the 3^1A^- diabatic state plays a predominant role in the reaction and that the 2^1A^- state is not the driving state but rather a spectator one. Namely, in contrast to the 2^1A^- state, which exhibits no reduction of electron density on the breaking bond and consequently could hardly descend in energy by C_1-C_6 bond stretching, the 3^1A^- state is a photochemically meaningful reactive state that can stabilize along the reaction path (compare Figures 2 and 3). We consider these findings as a step toward the full understanding of the ring-opening reaction in CHD and believe that the reinterpretation of the electronic character of the reactive state in CHD may also be of relevance for other pericyclic photoreactions.

CONCLUSIONS

The photochemical ring-opening reaction of CHD to HT is a textbook example of a pericyclic reaction and possibly the most investigated isomerization reaction with advanced time-resolved spectroscopies. Here, we provide a new insight into the mechanism of the reaction. In particular, we show that the doubly excited dark state, labeled 2^1A^-, which is considered in the literature as the gateway to the isomerization process, does not play a significant role. Instead, an initially high-lying state, labeled 3^1A^-, with a pronounced double excitation character and a significant reduction of electron density upon the C_1-C_6 bond (the one which breaks during the isomerization process), is the reactive state whose temporal evolution drives the reaction.

METHODS

Experimental Section. The experiments were performed at the LDM beamline[44] at the FERMI FEL facility. The Ti/sapphire optical laser (pump) was operated at 267 nm, with a bandwidth of 1.2 nm. The FEL pulse (probe) was set at a photon energy of 19.23 eV, corresponding to the fourth harmonic of the seed wavelength of 258 nm. The spectrometer used to collect photoelectrons was a magnetic bottle.[45,46] Electron time-of-flight (TOF) spectra were recorded shot-by-shot, while the delay between the pump and probe pulses was scanned with a step of 100 fs. The data used to construct Figure 1 consist of 15,000 shots per each delay, which were summed and normalized by the summed FEL intensity, recorded simultaneously for every shot. The electron flight times were converted to electron kinetic energies and calibrated according to ref 53 with respect to the FEL photon energy. The influence of the FEL and UV intensity on the TOF spectral shape was verified by performing a set of measurements at varied pulse energies and UV focus values. The third harmonic of the SLU at 267 nm has an estimated pulse duration of 120−170 fs, and the fourth harmonic of FERMI at 19.23 eV has an estimated pulse duration of ∼100 fs. A fwhm of 240 fs was used in the simulations, corresponding to a conservative evaluation of the overall time resolution. See Supporting Information for further details of experimental parameters, sample handling, and data analysis.

Computational Section. In all calculations, CHD and HT were described by extended multistate complete active space self-consistent field second-order perturbation theory (XMS-CASPT2),[68,69] employing an active space of six electrons in six orbitals, CAS[6e, 6o] (see Figure S7). In nonadiabatic dynamics simulations, the CASSCF orbitals were averaged over three states with equal weights. The three lowest electronic states of the CHD/HT cation (D_0, D_1, and D_2) were taken into account in the computation of the photoelectron spectra. The cc-pVDZ basis set was used in all computations, and a real shift of 0.5 Hartree was employed to avoid intruder states in the dynamics. All electronic structure calculations were performed with the BAGEL program.[70,71]

The photoelectron spectra were computed using the classical limit of the doorway−window formalism.[72,73] Nonadiabatic dynamics simulations were performed with Tully's fewest switches surface hopping algorithm[47] using an in-house code. The initial conditions were selected from the classical doorway function describing the excitation of the system by the pump pulse in our experiment.

Diabatic states were obtained from the adiabatic states by employing the diabatization scheme of Simah, Hartke, and Werner.[59]

https://doi.org/10.1021/jacs.2c06296
J. Am. Chem. Soc. 2022, 144, 21878−21886

To obtain smooth diabatic potentials, we included seven states in the calculations (XMS(7)-CASPT2[6e, 6o]). Details of the nonadiabatic dynamics simulations, the computation of photoelectron spectra, and the diabatization procedure are given in the Supporting Information.

■ ASSOCIATED CONTENT

Supporting Information

The Supporting Information is available free of charge at https://pubs.acs.org/doi/10.1021/jacs.2c06296.

Details regarding experimental setup and measurements on FERMI and the data analysis; details regarding the overall computational methodology, including static multireference calculations, nonadiabatic dynamics, spectrum calculation, and diabatization; and results that complement those presented in the article (PDF)

■ AUTHOR INFORMATION

Corresponding Authors

Nađa Došlić − *Institut Ruđer Bošković, Zagreb HR-10000, Croatia;* orcid.org/0000-0001-6535-9020; Email: nadja.doslic@irb.hr

Maria Novella Piancastelli − *Sorbonne Université, CNRS, Laboratoire de Chimie Physique-Matière et Rayonnement, LCPMR, Paris F-75005, France; Department of Physics and Astronomy, Uppsala University, Uppsala SE-751 20, Sweden;* orcid.org/0000-0003-3303-7494; Email: maria-novella.piancastelli@sorbonne-universite.fr

Authors

Oksana Travnikova − *Sorbonne Université, CNRS, Laboratoire de Chimie Physique-Matière et Rayonnement, LCPMR, Paris F-75005, France*

Tomislav Piteša − *Institut Ruđer Bošković, Zagreb HR-10000, Croatia*

Aurora Ponzi − *Institut Ruđer Bošković, Zagreb HR-10000, Croatia*

Marin Sapunar − *Institut Ruđer Bošković, Zagreb HR-10000, Croatia;* orcid.org/0000-0002-5717-1930

Richard James Squibb − *Department of Physics, University of Gothenburg, Gothenburg SE-412 96, Sweden*

Robert Richter − *Elettra-Sincrotrone Trieste, Trieste 34149, Italy*

Paola Finetti − *Elettra-Sincrotrone Trieste, Trieste 34149, Italy*

Michele Di Fraia − *Elettra-Sincrotrone Trieste, Trieste 34149, Italy*

Alberto De Fanis − *European XFEL, Schenefeld D-22869, Germany*

Nicola Mahne − *IOM-CNR, Trieste 34149, Italy*

Michele Manfredda − *Elettra-Sincrotrone Trieste, Trieste 34149, Italy*

Vitali Zhaunerchyk − *Department of Physics, University of Gothenburg, Gothenburg SE-412 96, Sweden;* orcid.org/0000-0001-7302-7413

Tatiana Marchenko − *Sorbonne Université, CNRS, Laboratoire de Chimie Physique-Matière et Rayonnement, LCPMR, Paris F-75005, France*

Renaud Guillemin − *Sorbonne Université, CNRS, Laboratoire de Chimie Physique-Matière et Rayonnement, LCPMR, Paris F-75005, France*

Loic Journel − *Sorbonne Université, CNRS, Laboratoire de Chimie Physique-Matière et Rayonnement, LCPMR, Paris F-75005, France*

Kevin Charles Prince − *Elettra-Sincrotrone Trieste, Trieste 34149, Italy;* orcid.org/0000-0002-5416-7354

Carlo Callegari − *Elettra-Sincrotrone Trieste, Trieste 34149, Italy;* orcid.org/0000-0001-5491-7752

Marc Simon − *Sorbonne Université, CNRS, Laboratoire de Chimie Physique-Matière et Rayonnement, LCPMR, Paris F-75005, France*

Raimund Feifel − *Department of Physics, University of Gothenburg, Gothenburg SE-412 96, Sweden;* orcid.org/0000-0001-5234-3935

Piero Decleva − *Dipartimento di Scienze Chimiche e Farmaceutiche, Universitá di Trieste, Trieste I-34127, Italy;* orcid.org/0000-0002-7322-887X

Complete contact information is available at: https://pubs.acs.org/10.1021/jacs.2c06296

Author Contributions

○O.T. and T.P. contributed equally and are both first authors.

Notes

The authors declare no competing financial interest.

■ ACKNOWLEDGMENTS

The authors are grateful to the FERMI team and laser group, in particular to L. Giannessi, M. B. Danailov, and A. Demidovich, for their continuous support during the experiments. T.P., A.P., M.S., P.D., and N.D. thank the Croatian Science Foundation for financial support (IP-2016-06-1142 and IP-2020-02-9932). R.F. thanks the Swedish Research Council and the Knut and Alice Wallenberg Foundation for financial support. The authors acknowledge the support of the COST Action CA18222 (Attosecond Chemistry). Many fruitful discussions with J. H. D. Eland, W. Domcke, and A. Prlj are gratefully acknowledged.

■ ABBREVIATIONS

CHD	1,3-cyclohexadiene
HT	1,3,5-hexatriene
CoIn	conical intersection
FEL	free-electron laser
LDM	low density matter
ESA	excited-state absorption
FC	Franck−Condon
BAC*	extended bond-alternating coordinate

■ REFERENCES

(1) Deb, S.; Weber, P. M. The ultrafast pathway of photon-induced electrocyclic ring-opening reactions: the case of 1,3-cyclohexadiene. *Annu. Rev. Phys. Chem.* **2011**, *62*, 19−39.

(2) Arruda, B. C.; Sension, R. J. Ultrafast polyene dynamics: the ring opening of 1,3-cyclohexadiene derivatives. *Phys. Chem. Chem. Phys.* **2014**, *16*, 4439.

(3) Celani, P.; Ottani, M.; Olivucci, F.; Bernardi, S.; Robb, M. A. What happens during the picosecond lifetime of 2A1 cyclohexa-1,3-diene? A CAS-SCF study of the cyclohexadiene/hexatriene photochemical interconversion. *J. Am. Chem. Soc.* **1994**, *116*, 10141−10151.

(4) Merchán, M.; et al. Electronic spectra of 1,4-cyclohexadiene and 1,3-cyclohexadiene: a combined experimental and theoretical investigation. *J. Phys. Chem. A* **1999**, *103*, 5468−5476.

(5) Garavelli, M.; et al. Reaction path of a sub-200 fs photochemical electrocyclic reaction. *J. Phys. Chem. A* **2001**, *105*, 4458−4469.

(6) Nenov, A.; Kölle, P.; Robb, M. A.; de Vivie-Riedle, R. Beyond the van der Lugt/Oosterhoff model: When the conical intersection seam and the S_1 minimum energy path do not cross. *J. Org. Chem.* **2010**, *75*, 123−129.

(7) Hofmann, A.; de Vivie-Riedle, R. Quantum dynamics of photoexcited cyclohexadiene introducing reactive coordinates. *J. Chem. Phys.* **2000**, *112*, 5054−5059.
(8) Schönborn, J. B.; Sielk, J.; Hartke, B. Photochemical ring-opening of cyclohexadiene: Quantum wavepacket dynamics on a global ab initio potential energy surface. *J. Phys. Chem. A* **2010**, *114*, 4036−4044.
(9) Ohta, A.; Kobayashi, O.; Danielache, S. O.; Nanbu, S. Nonadiabatic ab initio molecular dynamics of photoisomerization reaction between 1,3-cyclohexadiene and 1,3,5-cis-hexatriene. *Chem. Phys.* **2015**, *459*, 45−53.
(10) Lei, Y.; Wu, H.; Zheng, X.; Zhai, G.; Zhu, C. Photo-induced 1,3-cyclohexadiene ring opening reaction: Ab initio on-the-fly nonadiabatic molecular dynamics simulation. *J. Photochem. Photobiol. Chem.* **2016**, *317*, 39−49.
(11) Schalk, O.; et al. Cyclohexadiene revisited: A time-resolved photoelectron spectroscopy and ab initio study. *J. Phys. Chem. A* **2016**, *120*, 2320−2329.
(12) Polyak, I.; Hutton, L.; Crespo-Otero, R.; Barbatti, M.; Knowles, P. J. Ultrafast photoinduced dynamics of 1,3-cyclohexadiene using XMS-CASPT2 surface hopping. *J. Chem. Theory Comput.* **2019**, *15*, 3929−3940.
(13) Filatov, M.; Min, S. K.; Kim, K. S. Non-adiabatic dynamics of ring opening in cyclohexa-1,3-diene described by an ensemble density-functional theory method. *Mol. Phys.* **2019**, *117*, 1128−1141.
(14) Kotur, M.; Weinacht, T.; Pearson, B. J.; Matsika, S. Closed-loop learning control of isomerization using shaped ultrafast laser pulses in the deep ultraviolet. *J. Chem. Phys.* **2009**, *130*, 134311.
(15) Attar, A. R.; et al. Femtosecond x-ray spectroscopy of an electrocyclic ring-opening reaction. *Science* **2017**, *356*, 54−59.
(16) Adachi, S.; Sato, M.; Suzuki, T. Direct observation of ground-state product formation in a 1,3-cyclohexadiene ring-opening reaction. *J. Phys. Chem. Lett.* **2015**, *6*, 343−346.
(17) Pemberton, C. C.; Zhang, Y.; Saita, K.; Kirrander, A.; Weber, P. M. From the (1B) spectroscopic state to the photochemical product of the ultrafast ring-opening of 1,3-cyclohexadiene: A spectral observation of the complete reaction path. *J. Phys. Chem. A* **2015**, *119*, 8832−8845.
(18) Petrović, V. S.; et al. Transient X-ray fragmentation: probing a prototypical photoinduced ring opening. *Phys. Rev. Lett.* **2012**, *108*, 253006.
(19) Wolf, T. J. A.; et al. The photochemical ring-opening of 1,3-cyclohexadiene imaged by ultrafast electron diffraction. *Nat. Chem.* **2019**, *11*, 504−509.
(20) Karashima, S.; et al. Ultrafast ring-opening reaction of 1,3-cyclohexadiene: identification of nonadiabatic pathway via doubly excited state. *J. Am. Chem. Soc.* **2021**, *143*, 8034−8045.
(21) Minitti, M. P.; et al. Imaging Molecular Motion: Femtosecond X-Ray Scattering of an Electrocyclic Chemical Reaction. *Phys. Rev. Lett.* **2015**, *114*, 255501.
(22) Kosma, K.; Trushin, S. A.; Fuß, W.; Schmid, W. E. Cyclohexadiene ring opening observed with 13 fs resolution: coherent oscillations confirm the reaction path. *Phys. Chem. Chem. Phys.* **2009**, *11*, 172−181.
(23) Havinga, E.; Schlatmann, J. L. M. A. Remarks on the specificities of the photochemical and thermal transformations in the vitamin D field. *Tetrahedron* **1961**, *16*, 146−152.
(24) Anderson, N. A.; Shiang, J. J.; Sension, R. J. Subpicosecond ring opening of 7-dehydrocholesterol studied by ultrafast spectroscopy. *J. Phys. Chem. A* **1999**, *103*, 10730−10736.
(25) Matsuda, K.; Irie, M. Diarylethene as a photoswitching unit. *J. Photochem. Photobiol. C Photochem. Rev.* **2004**, *5*, 169−182.
(26) Kobatake, S.; Takami, S.; Muto, H.; Ishikawa, T.; Irie, M. Rapid and reversible shape changes of molecular crystals on photo-irradiation. *Nature* **2007**, *446*, 778−781.
(27) Irie, M.; Fukaminato, T.; Matsuda, K.; Kobatake, S. Photochromism of diarylethene molecules and crystals: memories, switches, and actuators. *Chem. Rev.* **2014**, *114*, 12174−12277.
(28) Dattler, D.; et al. Design of collective motions from synthetic molecular switches, rotors, and motors. *Chem. Rev.* **2020**, *120*, 310−433.
(29) Baroncini, M.; Silvi, S.; Credi, A. Photo- and redox-driven artificial molecular motors. *Chem. Rev.* **2020**, *120*, 200−268.
(30) Woodward, R. B.; Hoffmann, R. The conservation of orbital symmetry. *Angew. Chem., Int. Ed.* **1969**, *8*, 781−853.
(31) van der Lugt, W. T. A. M.; Oosterhoff, L. J. Quantum-chemical interpretation of photo-induced electrocyclic reactions. *Chem. Commun.* **1968**, 1235−1236.
(32) Van der Lugt, W. T. A. M.; Oosterhoff, L. J. Symmetry control and photoinduced reactions. *J. Am. Chem. Soc.* **1969**, *91*, 6042−6049.
(33) Pariser, R. Theory of the electronic spectra and structure of the polyacenes and of alternant hydrocarbons. *J. Chem. Phys.* **1956**, *24*, 250−268.
(34) Nakayama, K.; Nakano, H.; Hirao, K. Theoretical study of the $\pi\rightarrow\pi^*$ excited states of linear polyenes: The energy gap between $1^1B_u^+$ and $2^1A_g^-$ states and their character. *Int. J. Quantum Chem.* **1998**, *66*, 157−175.
(35) Domcke, W.; Yarkony, D. R.; Köppel, H.*Conical Intersections: Theory, Computation and Experiment*; World Scientific: Singapore, 2011.
(36) Nakamura, H.*Nonadiabatic Transition: Concepts, Basic Theories and Applications*; World Scientific: Singapore, 2012.
(37) Yarkony, D. R. Nonadiabatic quantum chemistry—past, present, and future. *Chem. Rev.* **2012**, *112*, 481−498.
(38) Domcke, W.; Stock, G. Theory of ultrafast nonadiabatic excited-state processes and their spectroscopic detection in real time. *Adv. Chem. Phys.* **1997**, *100*, 1−169.
(39) Shu, Y.; Varga, Z.; Kanchanakungwankul, S.; Zhang, L.; Truhlar, D. G. Diabatic States of Molecules. *J. Phys. Chem. A* **2022**, *126*, 992−1018.
(40) Ashfold, M. N. R.; Cronin, B.; Devine, A. L.; Dixon, R. N.; Nix, M. G. D. The Role of $\pi\sigma^*$ Excited States in the Photodissociation of Heteroaromatic Molecules. *Science* **2006**, *312*, 1637−1640.
(41) Scutelnik, V.; et al. X-ray transient absorption reveals the 1Au ($n\pi^*$) state of pyrazine in electronic relaxation. *Nat. Commun.* **2021**, *12*, 5003.
(42) Squibb, R. J.; et al. Acetylacetone photodynamics at a seeded free electron laser. *Nat. Commun.* **2018**, *9*, 63.
(43) Pathak, S.; et al. Tracking the ultraviolet-induced photochemistry of thiophenone during and after ultrafast ring opening. *Nat. Chem.* **2020**, *12*, 795−800.
(44) Svetina, C.; et al. The low density matter (LDM) beamline at FERMI: optical layout and first commissioning. *J. Synchrotron Radiat.* **2015**, *22*, 538−543.
(45) Eland, J. H. D.; et al. Complete two-electron spectra in double photoionization: the rare gases Ar, Kr, and Xe. *Phys. Rev. Lett.* **2003**, *90*, 053003.
(46) Eland, J. H. D.; Linusson, P.; Mucke, M.; Feifel, R. Homonuclear site-specific photochemistry by an ion−electron multi-coincidence spectroscopy technique. *Chem. Phys. Lett.* **2012**, *548*, 90−94.
(47) Tully, J. Molecular dynamics with electronic transitions. *J. Chem. Phys.* **1990**, *93*, 1061.
(48) Hanelli, R.; et al. Ab Initio Molecular Dynamics and Time-Resolved Photoelectron Spectroscopy of Electronically Excited Uracil and Thymine. *J. Phys. Chem. A* **2007**, *111*, 8500−8508.
(49) Tao, H.; et al. Ultrafast internal conversion in ethylene. I. The excited state lifetime. *J. Chem. Phys.* **2011**, *134*, 244306.
(50) Glover, W. J.; et al. Excited state non-adiabatic dynamics of the smallest polyene, trans 1,3-butadiene. II. Ab initio multiple spawning simulations. *J. Chem. Phys.* **2018**, *148*, 164303.
(51) Toffoli, D.; Stener, M.; Fronzoni, G.; Decleva, P. Convergence of the multicenter B-spline DFT approach forthe continuum. *Chem. Phys.* **2002**, *276*, 25−43.
(52) Ponzi, A.; Sapunar, M.; Angeli, C.; Cimiraglia, R.; Došlić, N.; Decleva, P. Photoionization of furan from the ground and excited electronic states. *J. Chem. Phys.* **2016**, *144*, 084307.

https://doi.org/10.1021/jacs.2c06296
J. Am. Chem. Soc. 2022, 144, 21878−21886

(53) Kimura, K.et al.*Handbook of HeI Photoelectron Spectra of Fundamental Organic Molecules*; Japan Scientific Societies Press: Tokyo, 1981; p 68.
(54) Beez, M.; Bieri, G.; Bock, H.; Heilbronner, E. The Ionization Potentials of Butadiene, Hexatriene, and their Methyl Derivatives: Evidence for through space interaction between double bond ?-orbitals and non-bonded pseudo-? orbitals of methyl groups? *Helv. Chim. Acta* **1973**, *56*, 1028−1046.
(55) Robin, M. B.*Higher Excited States of Polyatomic Molecules*; Academic Press: New York, 1975; Vol. *2*.
(56) McDiarmid, R.; Sabljić, A.; Doering, J. P. Valence transitions in 1,3-cyclopentadiene, 1,3-cyclohexadiene, and 1,3-cycloheptadiene. *J. Chem. Phys.* **1985**, *83*, 2147−2152.
(57) Ning, J.; Truhlar, D. G. The valence and Rydberg states of dienes. *Phys. Chem. Chem. Phys.* **2020**, *22*, 6176−6183.
(58) Mori, T.; Glover, W. J.; Schuurman, M. S.; Martinez, T. J. Role of Rydberg States in the Photochemical Dynamics of Ethylene. *J. Phys. Chem. A* **2012**, *116*, 2808−2818.
(59) Simah, D.; Hartke, B.; Werner, H.-J. Photodissociation dynamics of H2S on new coupled ab initio potential energy surfaces. *J. Chem. Phys.* **1999**, *111*, 4523−4534.
(60) Garavelli, M.; Celani, P.; Fato, M.; Bearpark, M. J.; Smith, B. R.; Olivucci, M.; Robb, M. A. Relaxation Paths from a Conical Intersection: The Mechanism of Product Formation in the Cyclohexadiene/Hexatriene Photochemical Interconversion. *J. Phys. Chem. A* **1997**, *101*, 2023−2032.
(61) Celani, P.; Bernardi, F.; Robb, M. A.; Olivucci, M. Do Photochemical Ring-Openings Occur in the Spectroscopic State? $^1B_2$ Pathways for the Cyclohexadiene/Hexatriene Photochemical Interconversion. *J. Phys. Chem.* **1996**, *100*, 19364−19366.
(62) Tamura, H.; Nanbu, S.; Nakamura, H.; Ishida, T. A theoretical study of cyclohexadiene/hexatriene photochemical interconversion: multireference configuration interaction potential energy surfaces and transition probabilities for the radiationless decays. *Chem. Phys. Lett.* **2005**, *401*, 487−491.
(63) Hofmann, A.; de Vivie-Riedle, R. Adiabatic approach for ultrafast quantum dynamics mediated by simultaneously active conical intersections. *Chem. Phys. Lett.* **2001**, *346*, 299−304.
(64) Tamura, H.; Nanbu, S.; Ishida, T.; Nakamura, H. Ab initio nonadiabatic quantum dynamics of cyclohexadiene/hexatriene ultrafast photoisomerization. *J. Chem. Phys.* **2006**, *124*, 084313.
(65) Coonjobeeharry, J.; et al. Mixed-quantum-classical or fully-quantized dynamics? A unified code to compare methods. *Philos. Trans. R. Soc., A* **2022**, *380*, 20200386.
(66) Kim, J.; Tao, H.; Martinez, T. J.; Bucksbaum, P. Ab Initio Multiple Spawning on Laser-Dressed States: A Study of 1,3-Cyclohexadiene Photoisomerization via Light-Induced Conical Intersections. *J. Phys. B: At., Mol. Opt. Phys.* **2015**, *48*, 164003.
(67) Kim, J.; Tao, H.; White, J. L.; Petrović, V. S.; Martinez, T. J.; Bucksbaum, P. H. Control of 1,3-Cyclohexadiene Photoisomerization Using Light-Induced Conical Intersections. *J. Phys. Chem. A* **2012**, *116*, 2758−2763.
(68) Shiozaki, T.; Győrffy, W.; Celani, P.; Werner, H.-J. Communication: Extended multi-state complete active space second-order perturbation theory: Energy and nuclear gradients. *J. Chem. Phys.* **2011**, *135*, 081106.
(69) Park, J. W.; Shiozaki, T. On-the-fly CASPT2 surface-hopping dynamics. *J. Chem. Theory Comput.* **2017**, *13*, 3676−3683.
(70) Shiozaki, T. BAGEL: Brilliantly advanced general electronicstructure library. *Wiley Interdiscip. Rev.: Comput. Mol. Sci.* **2018**, *8*, No. el1311.
(71) Shiozaki Group. BAGEL: Brilliantly Advanced General Electronic-structure Library. http://www.nubakery.org (accessed on Nov 3, 2022).
(72) Gelin, M. F.; et al. Ab initio surface-hopping simulation of femtosecond transient-absorption pump−probe signals of non-adiabatic excited-state dynamics using the doorway−window representation. *J. Chem. Theory Comput.* **2021**, *17*, 2394−2408.
(73) Piteša, T.; et al. Combined Surface-Hopping, Dyson Orbital, and B-Spline Approach for the Computation of Time-Resolved Photoelectron Spectroscopy Signals: The Internal Conversion in Pyrazine. *J. Chem. Theory Comput.* **2021**, *17*, 5098−5109.

https://doi.org/10.1021/jacs.2c06296
J. Am. Chem. Soc. 2022, 144, 21878−21886